International Soil and Water Conservation Research 11 (2023) 494–506

Contents lists available at ScienceDirect

International Soil and Water Conservation Research

journal homepage: www.elsevier.com/locate/iswcr

Original Research Article

Novel sediment source fingerprinting quantifying erosion-induced total nitrogen and total phosphorus outputs from an intensive agricultural catchment, North China

Hanqing Yu [a, *], Joseph Adu-Gyamfi [b], Suarau Odutola Oshunsanya [a, c], Adrian Chappell [d], Wenxiang Liu [a, e], Yu Zheng [a], Tingting Xue [a], Lee Heng [b]

[a] Agricultural Clean Watershed Research Group, Institute of Environment and Sustainable Development in Agriculture, Chinese Academy of Agricultural Sciences (CAAS), Haidian District, 100081, Beijing, China
[b] International Atomic Energy Agency, Vienna, Austria
[c] Department of Agronomy, University of Ibadan, Nigeria
[d] School of Earth and Environmental Sciences, Cardiff University, Cardiff, UK
[e] Chongqing Branch Institute, Changjiang River Scientific Research Institute, Chongqing, 400026, China

ARTICLE INFO

Article history:
Received 14 June 2022
Received in revised form
9 October 2022
Accepted 19 October 2022
Available online 31 October 2022

ABSTRACT

Intensive farming is a primary cause of increased sediment and associated nitrogen (N) and phosphorus (P) loads in surface water systems. Determining their contributing sources, pathways and loads present major challenges in the high-intensity agricultural catchments. Herein, we quantify the sediment sources and magnitude of sediment total N and total P from different sources using a novel application of compound-specific stable isotope (CSSI) and fallout radionuclides (FRNs) of ^{137}Cs and ^{210}Pbex in an intensive agricultural catchment in North China. Sediment sources from surface and sub-surface soils were estimated from FRNs fingerprint and accounted for 62 ± 7% and 38 ± 7% respectively, while surface soil from land uses that originated from hillslope were identified by CSSI fingerprint. Using a novel application of FRNs and CSSI sediment fingerprinting techniques, the dominant sediment source was derived from maize farmland (44 ± 0.1%), followed by channel bank (38 ± 7%). The sedimentation rate (13.55 ± 0.30 t ha^{-1} yr^{-1}) was quantified by the ^{137}Cs cores (0–60 cm) at the outlet of this catchment. The total N and total P in sediment were both mostly derived from maize farmland and least from channel banks. The channel banks are significant sediment sources but contribute little to the input of sediment N and P for eutrophication. It implies that chemically-applied farmlands are the main hotspots for catchment erosion control and pollution prevention. The novel application of FRNs and CSSI techniques cost-effectively quantified sediment N and P loads from different sources with a single visit to the catchment, enabling rapid assessment for optimizing soil conservation strategies and land management practices. Keywords: Sediment sources, Land use, N and P loads, Compound-specific stable isotope, Fallout radionuclides.

1. Introduction

Increased population pressure and commercial agriculture in most countries have caused land use intensification (Mendoza-Fernández et al., 2021; Prabhakar, 2021; Xie et al., 2021). The main sources of agricultural non-point source pollution are chemical fertilizers and pesticides which are carried by sediment along runoff and discharged into surface water (Bai et al., 2020; Peris et al., 2022). Excessive N and P fertilizer application in agricultural uplands can also accelerate eutrophication (Rattan et al., 2017; Winogradow & Pempkowiak, 2020). As a consequence of loss of soil cover and intensive soil tillage, soil erosion on sloping lands was enhanced resulting in associated soil degradation through removing nutrient-rich topsoil (e.g., total N and total P)

* Corresponding author.
E-mail address: yuhanqing@caas.cn (H. Yu).

https://doi.org/10.1016/j.iswcr.2022.10.006

from uplands to lowlands (Bai et al., 2020; Quinton et al., 2010). This accelerated soil erosion increased sediment and N and P loads in rivers and local reservoirs. Consequently, the increasing soil erosion by intensified agricultural practices and associated N and P contaminants lead to environmental and water pollution (Robotham et al., 2021; Wang et al., 2021).

To counteract this development and to design soil conservation measures at designated soil erosion hot spots, accurate analytical methods are required to trace predominant sources in sediment and associated N and P by soil erosion from different land uses. Sediment source tracing refers to a field-based measurement technique that apportions or un-mixes sediment samples into multiple sources through the use of tracers (Collins et al., 2017, 2020; Haddadchi et al., 2013; Nosrati et al., 2021; Owens et al., 2016; Walling, 2013). Tracers used in sediment fingerprinting studies include color parameters (García-Comendador et al., 2020), plant pollen (Kobe et al., 2021), major and trace elemental composition (Li et al., 2019), rare earth elements (Astakhov et al., 2019; Brito et al., 2018), mineral magnetic characteristics (Wei et al., 2021), clay mineralogy (Verma et al., 2014) and E-DNA approach (Evrard et al., 2019). In particular, geochemical tracer techniques have been used to distinguish sediments in soils formed from different rock types (Gholami et al., 2019; Huang et al., 2020; Li, Gholami, et al., 2020; Nosrati et al., 2021; Torres Astorga et al., 2020).

In addition, fallout radionuclides (FRNs, e.g., caseum-137, ^{137}Cs and excess lead-210, ^{210}Pbex) have been widely used to determine the relative contributions of surface and sub-surface soil erosion to stream sediments (Hancock et al., 2014; Nosrati, 2017; Olley et al., 2013; Smith & Blake, 2014). This approach is based on the principle of FRNs being concentrated in the surface soil. Sediments eroded from the soil surface will have large concentrations of radionuclides, whereas sediment eroded from gullies, channels or other sub-surface sources have small concentrations (Olley et al., 2013). Radionuclide tracers may also provide a sound physical basis for discrimination between cultivated land and uncultivated land sources (Smith & Blake, 2014), and also can be used to determine soil redistribution and sediment yield due to different land use types or management changes (Mabit et al., 2009). However, the sediment contribution of different specific plant species to reservoir sediment cannot be identified using radionuclide tracers (Reiffarth et al., 2016).

Compound-specific stable isotope (CSSI) technique based on the use of the carbon-13 (δ^{13}C) stable isotope signature of fatty acids (FA) or alkanes (in soils and sediments) can be implemented to apportion land-use-specific sediment sources driven by soil erosion across landscapes (Alewell et al., 2016; Blake et al., 2012; Brandt et al., 2016; Bravo-Linares et al., 2018; Gibbs et al., 2020; Hancock & Revill, 2013; Hirave et al., 2020; Mabit et al., 2018; Upadhayay et al., 2018). The CSSI technique was first introduced to study the origin of estuarine sediments in 2008 (Gibbs, 2008). The main principles of the technique are that the compounds (e.g. FA) produced by plants can be used as labels or “biomarkers” for a specific type of soil (land use). The CSSI-based fingerprinting involves carbon isotope ratio measurements of compounds of interest from source soils, suspended or riverbed sediments from rivers or lakes (as mixture). The source proportions in the mixture are computed using end-member mixing models, including IsoSource which is based on frequentist inference (Phillips & Gregg, 2003) or Bayesian approaches such as SIAR, MixSIAR (Stock & Semmens, 2018). However, the above traditional methods, such as geochemical, biomarker fingerprinting and single stable isotope or FRNs technology cannot quantitatively identify the source and load of agricultural non-point source pollutants (total N and total P) in reservoir sediment.

North China is characterized by high-intensity agricultural activities for commercial wheat and maize production. The intensive farming in North China accounts for more than 17% of China's arable land area. With rapid development of intensive agricultural production systems, large inputs of synthetic N and P fertilizer and decreasing N and P use efficiency have led to a series of aquatic environmental problems (Selman & Greenhalgh, 2010). The depressions intercept runoff pollution and sediments containing pollutants are deposited. The sedimentary process of deposition of N and P pollutants from different sediment sources are bound to vary. Although some studies have reported on speciation and distribution of the nutrients (N and P) in river/lake sediment (Li et al., 2012; Shen et al., 2021), the effect of agricultural intensification on historical nutrient dynamics and source in the sediments (Ni et al., 2015), estimating the flux loads and sources of total N (TN) and total P (TP) by hydrologic surveys and an experimental simulation of suspended sediment (Wang et al., 2017), finding the source and major factors of estuarine sediment N loading by model (Li, Zhao, et al., 2020), identifying recent sources and fate of sedimentary N in the Baltic Sea based on organic matter elemental composition and N and carbon (C) stable isotopes ratios (Winogradow & Pempkowiak, 2020), and identifying sources and cycling of P in the sediment of inflow rivers (Wang et al., 2021), no information is available about quantitively identifying N and P pollutants-based sediment sources under different land management.

Thus, the objectives of this study were to (1) identify the relative contributions of sources from different land use types and subsurface soils to the sediment deposited, and (2) quantify the sediment total N and total P loads exported from the different sediment sources in an intensive agricultural catchment in North China. To the best of our knowledge, this is the first study to quantify sediment sources and associated total N and total P load outputs in an intensive agricultural catchment prone to human intervention by a novel application of CSSI and FRNs (^{137}Cs and ^{210}Pbex) tracer approaches. The results can provide better discrimination between sediment derived from surface soils and deeper layers, as well as quantitative information on sources and loads of N and P pollutants in sediment exported from different sources at the catchment scale, and will allow decision maker of land management to evaluate and improve land management practices to reduce pollution of the waterways of the region.

2. Materials and methods

2.1. Study site

The Jiangou catchment is located in the suburban of Beijing (40°48′0″N, 116°56′30″E), in the intensive farming area of North China. The climate is characterized by temperate semi-humid continental monsoon with a 40-year average rainfall of 610 mm per annum. About 80% of the annual precipitation in the region usually occurs between June and August. Annual rainfall normally varies from one year to another. The average annual temperature is 12 °C, with a maximum of 26 °C in July and a minimum of −6 °C in January. The catchment covers a total area of 13.85 km^2 and has an altitudinal range of <20–114 m above sea level (a.s.l.). The terrain gradually slopes from northwest to southeast and with a gentle slope of 3°–10°. Some small streams gather at the only outlet in the low-lying area of the catchment and eventually flow into the Ju River, which is the tributary of Haihe River, one of the seven major rivers in China.

Land use types in the catchment were interpreted by Google Earth and field surveys. The area of each land use type is calculated using the “Spatial Analyst Tool” by ArcGIS. Characteristic land use types of the catchment surrounding the mainstream included

residences, rock hilly area, dairy farm built-up area, maize (*Zea mays* L.) farmland, mung bean (*Vigna radiata (L.) Wilczek*) farmland, vegetable such as cabbage (*Brassica oleracea* L.) and broccoli (*Brassica oleracea* L. *var.italic Planch.*) farmland and forest such as Populus alba (*Populus tomentosa Carr*) and red maple (*Acer palmatum 'Atropurpureum'*). Forest land accounts for the largest area of 39%, followed by the residences (18%) and maize farmland (14%), the rock hilly area, dairy farm built-up area, bean and vegetable farmlands were the least, accounting for 5%, 5%, 9% and 8%, respectively (Fig. 1a). Compound NPK fertilizer with 15% total N, 15% P_2O_5, 15% K_2O was used for maize farmland in April and/or June and again in September (some are rotated with winter wheat). Vegetable and bean farmlands were mainly fertilized with organic manure (750 kg ha^{-1} applied three times per year).

The river channels of the main stream and major tributary in this catchment are mostly repaired based on their self-formed formation, and some of the river channel banks in this catchment have been made by people using stones or cement. We conducted a field survey on the number and morphological indicators of "natural channel banks" which were not built with stone or cement within the catchment, and calculated these "natural channel banks" areas within the whole catchment (see Table S1).

2.2. Sample collection

In 2019 September, based on the field survey, catchment characteristics and sediment connectivity map (Fig. 1b) which is an alternative line of evidence for field survey to determine erosion hotspots, five major sediment sources (maize farmland, bean farmland, vegetable farmland, forest land and channel bank) were identified as major contributors to the sedimentation process in this catchment. Sediment connectivity is defined as the degree of linkage between sediment sources, downstream areas and sediment collection location in a freshwater system (Borselli et al., 2008; Cavalli et al., 2013). Using ZY-3 Satellite DEM (5 m solution, made by Suzhou Zhongke Tianqi Remote Sensing Technology Co., Ltd., Pixel Grid SAT software) and land use map of the catchment, the index of sediment connectivity (IC) was calculated as given by Cavalli et al. (2013). In addition to topography, a weighing factor was also introduced to compute the IC to model the impedance of

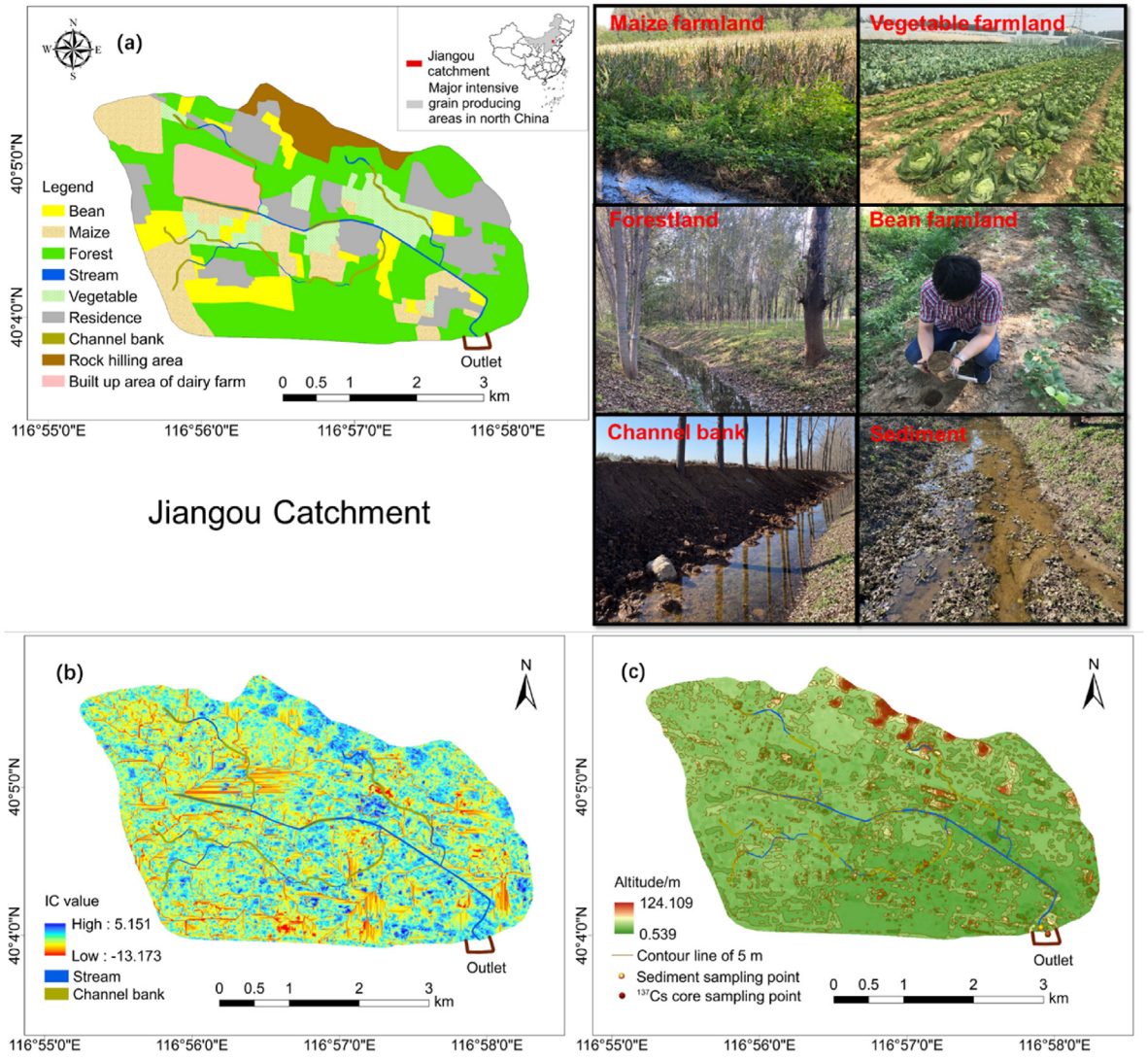

Fig. 1. Study catchment. (a) Location, land uses, sediment sources landscapes and deposited sediment of study catchment within the major Grain Production area with intensive agricultural practices in North China; (b) Sediment connectivity map of this catchment based on Cavalli et al. (2013) and (c) Contour map of this catchment, river bed sediment sampling location (yellow dot) and ^{137}Cs core sampling location (red dot).

runoff and sediment fluxes due to the properties of local land use. We used the vegetation cover factor of the universal soil loss equation (C-Factor) as the connectivity weighting factor (W), the W values vary from 0 to 1, with values close to 0 assigned in case of characteristics that inhibit (reduce the connection) water and sediment transfer, such as forest. Values close to 1 correspond to those land uses that permit (favor the connection) the passage of water and sediment, such as bare soil. (Borselli et al., 2008). Here, we did not consider the dairy farm as a potential source because this dairy farm is a dairy factory built-up area, the sediment connectivity values of this area were also very low which corroborated the fact that the sediment flowing into the channel from the dairy farm is very limited due to the built-up area which is a flat concrete environment.

The ^{137}Cs and ^{210}Pbex soil sampling was conducted from the surface (0–2 cm) and sub-surface soils for sediment source fingerprinting. For the sub-surface soils i.e. "natural channel banks" in this catchment as described in section 2.1, they were considered as original separate sources to river sediment and did not use vegetation-specific tracer to distinguish it since these channel bank soils did not contain any plant component materials after man-made construction. The cutting samples were collected by scraping soil from the full vertical extent of actively eroding bank face materials, to ensure that only sediments from the channel bank were sampled. 6 composited soil samples were obtained from 20 subsamples for each composited sample along the channel bank.

The surface soils were sampled from each different major land use that has the potential to erode and the areas that are easily connected to the mainstream. The topsoil (0–2 cm) sampling for CSSI and ^{137}Cs and ^{210}Pbex was conducted to represent different land use types (plant species) and the primary topographic settings in the surface soil area (i.e., hillslope surface soil). For each land use type, samples were collected from scattered plots with the area of 100 m^2 for each plot. Thereafter, 20 subsamples were collected from each plot and mixed into a plastic bucket as one composited sample. To avoid potential cross-contamination in the samples and soil compositing, plastic gloves were used when mixing the soil samples and the plastic bucket was washed thoroughly between uses. The numbers of composite samples retrieved per source category of hillslope surface area were as follows: maize farmland (n = 9); bean farmland (n = 7); vegetable farmland (n = 8), and forest land (n = 11). These spatially-integrated mixtures allow us to get the true representative samples of each land use type and therefore a trade-off between the degree of spatial variability of CSSI values and analytical costs which are necessary to meet the research objectives.

The river bed sediment samples were collected from the surface of soil layers (0–2 cm) which have been transported downslope by runoff near the outlet of the catchment, following the above procedures to ensure a representative sample (Fig. 1c). A total of 7 composited sediment samples were collected.

To estimate sediment yield in the catchment, soil cores (the soil profiles 1 and 2) were collected at the outlet of the catchment, i.e. deposition area where there was abandoned cultivated land in recent years, at the depth of 0–60 cm with an increment of 5 cm using a hand-operated core sampler with a diameter of 6.7 cm, for ^{137}Cs activity analysis. Three different cores were collected in a radius of 2 m, the samples from similar depth increment were combined to obtain a composite profile, i.e. the profile 1 and 2. reference ^{137}Cs were also collected from undisturbed, uneroded and flat grassland which present more than 60 years near the study site. In total, we collected 8 undisturbed soil cores from the grassland to a depth of 45 cm to estimate the ^{137}Cs reference inventory, and 5 of those samples were divided into 9 sections with intervals of 5 cm to create layered composite samples.

2.2.1. Soil properties analysis

Soil bulk density (BD, g cm^{-3}) calculations were based on the volume of bulked soil cores and oven-dried soil mass determinations. Total N was determined by Kjeldahl digestion procedures (Bremner, 1960). Total P was analyzed using the ascorbic acid reduction procedures with a UV spectrophotometer (Sherrell & Saunders, 1966).

2.2.2. Measurement of soil ^{137}Cs and ^{210}Pb$_{ex}$

Soil samples were air-dried, ground and then passed through a 2 mm sieve prior to measuring the ^{137}Cs and ^{210}Pb$_{ex}$ activities (Pennock & Appleby, 2002). Soil samples for measuring ^{210}Pb were sealed in cylinder containers and stored for 28 days to ensure equilibrium between ^{226}Ra and its daughter ^{222}Rn (half-life 3.8 days). The amounts of ^{210}Pb$_{ex}$ in the samples were calculated by subtracting ^{226}Ra-supported ^{210}Pb concentration from the total ^{210}Pb concentrations. Measurement of the ^{137}Cs and ^{210}Pb activities were undertaken using a broad-energy hyper pure coaxial Ge (HPGe) detector with a relative detection efficiency of 50.9% (BE5030; Canberra Industries Inc., Meriden, CT, USA). The activity of ^{137}Cs was detected at 662 keV peak while the total ^{210}Pb concentration was determined at 46.5 keV, and the ^{226}Ra-supported ^{210}Pb was obtained at 609.3 keV using counting time over 80,000 s, which provided an analytical precision of ±5% for ^{137}Cs (Bq kg^{-1}) and ±8% for ^{210}Pb (Bq kg^{-1}) (Li et al., 2003).

2.3. Sedimentation rate estimation

Estimation of sediment production using ^{137}Cs involves the comparison of the measured inventories (total activity in the soil profile per unit area) at all sample sites in the depositional area at the outlet of the catchment with an estimate of the total atmospheric input obtained from the reference site. The excess inventory represents the input associated with deposited sediment and its magnitude will, therefore, reflect the rate of sediment deposition and the concentration in the deposited sediment. At each sampling point, the rate of sediment deposition was determined using the Mass Balance Model 2 (MBM 2) (Walling et al., 2002).

2.4. Bulk δ^{13}C and compound-specific stable isotope (CSSI)

The collected soil samples from the field were processed following Gibbs' (2014) protocol. The samples were dried in the oven at a temperature of 60 °C for 24 h. The samples were passed through a 100-mesh sieve and ground before acidifying 5 g of the sample with 5 ml of 10% hydrochloric acid to eliminate inorganic carbonates. The solution was transferred into a 50 ml plastic tube and centrifuged for 10 min. Thereafter, successive 2 ml aliquots of 10% hydrochloric acid were added to the solution with stirring, until the addition produced no fizzing. The solution was further centrifuged for another 10 min at 3000 rpm after diluting the solution with distilled water to 50 ml. The mixture was separated by decantation. The solid mixture was then washed with an additional 50 ml of distilled water. The wet acidified solid particles were oven dried at 60 °C before analysis of total organic carbon (%Corg) and δ^{13}C of the bulk soil on a Thermo Finnegan Delta Plus Isotope Ratio Mass Spectrometer following combustion at 1010 °C in an elemental analyzer.

A Dionex Accelerated Solvent Extraction (ASE 350 Thermo) was used to extract fatty acids from a non-acidified homogenized soil particle. Dichloromethane (DCM) at 100 °C under a pressure of 2000 psi was used to extract for 5 min, the extraction procedure was repeated twice (Gibbs et al., 2020). The collection vial is rinsed twice with a small volume (~5 ml) of DCM, and the solvent extract

was reduced to 2 ml in the 50 ml round-bottom rotary evaporator flask for evaporation using a Buchi rotary evaporator. The mixture was then transferred into a screw-cap test tube (20 ml) by adding DCM before air drying to 1 ml. Then 5 ml saponification solution (0.5 M KOH/MeOH/H_2O) was added and placed in a water bath at 40 °C overnight (Hu et al., 2006). The pH was adjusted to <2 by adding HCl, repeatedly adding 5 ml hexane/DCM (9: 1) five times, and the upper layer was transferred to the evaporator flask and then reduced to 1 ml under a stream of nitrogen gas. The extracted solution was passed through anhydrous sodium sulfate column into a 10 ml Kimax tube. The fatty acid methyl esters were obtained from fatty acid through methylation process. During the process, 2 ml of 5% of boron fluoride catalyst was added to a tube containing pure methanol and mixed with vortex for 1 min. The mixture was then sealed and heated up at 70 °C for 20 min in a water bath or a fan-ventilated oven. The supernatant was taken to the 4 ml vials after being extracted by hexane in tube more than 3 times. Then the mixture was reduced to 1 ml in a 2 ml vial under a stream of nitrogen gas before measuring fatty acid methyl esters by GC-IRMS (i.e., an Agilent 6890 gas chromatograph and a Thermo Delta V mass spectrometer). An HP-5 fused silica capillary column with 60 m × 0.25 mm and 0.25 μm film was employed to separate the fatty acid methyl esters into various components. Fatty acid methyl esters (FAMEs) were identified by retention times against external (C14:0, C16:0, C18:0, C20:0, C22:0, C24:0, C26:0, C28:0 and C30:0) and internal (eg. C19:0 FA) standards confirmed by GC-mass spectrometer analysis.

In addition, methanol employed for digestion was analyzed for $\delta^{13}C$ in order to amend the value of fatty acid methyl esters isotope for inclusion of methyl compound as presented in Eq. (1) (Gibbs, 2008).

$$\delta^{13}C_{FA} = \frac{\delta^{13}C_{FAME} - (1 - X)\delta^{13}C_{Methabol}}{X} \quad (1)$$

where FA, FAME and *X* represent fatty acid, fatty acid methyl esters and the contribution by the proportion of carbon atoms on FA to FAME basis, respectively. To estimate *X*, the number of carbons in the FA is divided by the number of carbon atoms present in the FAME. The analytical precision is estimated at 0.2‰.

2.5. Determining sediment sources

2.5.1. Proportion of surface and sub-surface sediment sources

The sediment sources were broadly divided into two categories: surface soil from hillslope and sub-surface soils from channel banks. Fallout radionuclides of the accumulated sediment from the two sediment sources are anticipated to be different, and a two-end-member mixing model was employed to determine the relative contributions of the two potential sediment sources to the sediment deposit as presented in Eq. (2) and Eq. (3).

$$f_{s1}C_{s1} + f_{s2}C_{s2} = C_m \quad (2)$$

$$f_{s1} + f_{s2} = 1 \quad (3)$$

where f_{s1} and f_{s2} represent the relative contributions from surface soil and sub-surface soil sources to the deposited sediment, respectively. C_{s1} and C_{s2} represent the activities of ^{137}Cs or $^{210}Pb_{ex}$ from surface soil and sub-surface soil sources, and C_m represents the respective total activities of ^{137}Cs or $^{210}Pb_{ex}$ of the deposited sediment.

To solve for f_{s1}, Eq. (4) is rewritten as:

$$f_{s1} = (C_m - C_{s2})/(C_{s1} - C_{s2}) \quad (4)$$

and for f_{s2}, Eq. (5) is rewritten as:

$$f_{s2} = (C_m - C_{s1})/(C_{s2} - C_{s1}) \quad (5)$$

^{137}Cs and $^{210}Pb_{ex}$ were used individually to run the models to obtain average surface and sub-surface soil contributions. Because each individual result is a unique solution, the mean and standard deviation about the mean of all of these results provide a statistical indication of the level of uncertainty in the result. Identification of valid feasible results from the full suite of two end-member mixing model results can be confirmed with the polygon test (Fig. S1) i.e. a straight line through all points (averaged surface soil, sub-surface soil and mixture sediment) indicating that both tracers can be used in the two end-member mixing model (IAEA, 2019). This result is reconfirmed by sediment mixtures analyses were within the range of ^{137}Cs and $^{210}Pbex$ values of all the sources (Fig. 2).

2.5.2. Mixing models used for apportioning different land use sources in sediment

The source contributions of the mixtures were estimated using a Bayesian isotope mixing model MixSIAR (Stock & Semmens, 2018) which was implemented as an open-source R package. The complete set of MixSIAR equations and additional explanation is

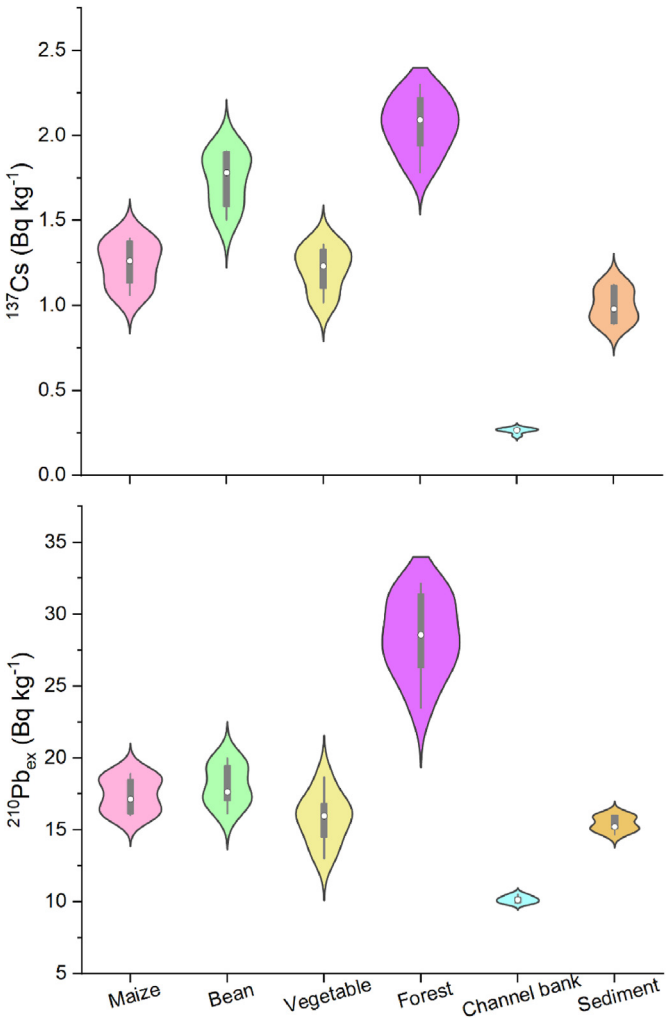

Fig. 2. The activity of ^{137}Cs and $^{210}Pb_{ex}$ under different land uses in the Jiangou catchment. The central box is extended from the 25–75 percentiles, the hollow circle is plotted at the median and whiskers show 5–95 percentile range.

included in Stock et al. (2018) and references therein. MixSIAR is a probabilistic Bayesian mixing model that generates a probability density function using a Markov Chain Monte Carlo (MCMC) method. It produces simulations of plausible values, therefore representing a true probability density function for the proportional contribution of source soils in the mixture being tested. In this study, bulk C $\delta^{13}C$ values for each end member plus $\delta^{13}C$ values for a range of selected fatty acids (C20:0, C22:0, C24:0 and C26:0) were inserted into the model to discriminate sources. The conservativeness of bulk ^{13}C and above carbon isotope composition ($\delta^{13}C$ values) of fatty acids was checked using the polygon test (Fig. S3). Concentration-dependent MixSIAR was formulated with selected FAs, using a residual error term and no prior information. The Markov chain Monte Carlo parameters were set as follows: number of chains = 3; chain length = 300,000; burn = 200,000; thin = 100. Convergence of the MixSIAR model was evaluated using the Gelman- Rubin diagnostic, and in our case none of the variables were >1.01, attaining the requirement of model convergence.

The outputs from Mixing Model, as it is used in the CSSI technique, are based on isotopic values of carbon and are given as carbon isotopic proportions, not soil proportions. As the isotopic biomarkers are a small fraction of the organic matter in the soil and the organic matter is typically less than 10% of the whole soil, the isotopic proportions must be converted to soil proportions ($Soilsource_n$, %). This conversion is done using a linear correction equation based on the carbon content of each source soil (Gibbs, 2008) as presented in Eq. (6).

$$\%Soilsource_n = \frac{P_n/\%C_n}{\sum_{n}^{i}(P_n/\%C_n)} \times 100 \quad (6)$$

where P_n (%) is the mean feasible proportion of source n in the mixture as estimated from isotopic values of carbon by Mixing Model, and $\%Cn$ is the % carbon in the source n soil. Because this calculation only uses the %C of the source soils for scaling, the proportional contribution of each source soil is independent of any loss of total carbon or fatty acids in the mixture through biodegradation.

2.6. Estimation of export load of sediment N and P from different sources in the catchment

Export load of sediment N and P (t yr^{-1}) were calculated according to Eq. (7) and Eq. (8).

$$EN_{LOAD\_n} = SR \times Soilsource_n \times C_{TN\_n} \times A_n \quad (7)$$

$$EP_{LOAD\_n} = SR \times Soilsource_n \times C_{TP\_n} \times A_n \quad (8)$$

where SR (t ha^{-1} yr^{-1}) is the sedimentation rate at the outlet of this catchment; C_{TN_n} (%) and C_{TP_n} (%) are TN and TP concentrations in source n soil samples for each land use; A_n (ha) denotes the area of source n.

2.7. Data processing and analysis

Sediment source ascription using CSSIs (e.g., FAMEs) requires that naturally abundant $\delta^{13}C$ values of FAMEs differ significantly between the source soils representing distinct land use types. Kruskal-Wallis Test was applied to determine these significant differences between $\delta^{13}C$ values of identical FAMEs among different source soils. The point-in-polygon test was employed to identify whether a proposed mixing model could generate a reliable mass balance for all potential erosion sources. Principal Component Analysis (scores and loadings) showing the distribution of the different isotopic signatures for the sources were determined using the R software package Vegan.

The novel combination of FRN and CSSI fingerprinting was employed to identify the apportionment of all sediment sources. Each land use type sediment source proportion was obtained by multiplying the proportion of hillslope surface soil in the sediment deposit using FRN fingerprint and the proportion of land use-based sediment source apportionment using CSSI fingerprint, and their standard deviation was determined using the multiplication error transfer method (Song, 1982).

3. Results

3.1. Fatty acid analysis of soil sources and discrimination of the most suitable FAs

The mean ± SD of $\delta^{13}C_{FA}$, bulk C $\delta^{13}C$ of signature and bulk C under each soil source on the surface soil area are summarized in Table 1. In general, there is no significant difference between $\delta^{13}C_{FA}$ for maize, bean and vegetable farmlands, but good discrimination between the $\delta^{13}C_{FA}$ values for them from forest soils. Maize, bean and vegetable soils showed the highest $\delta^{13}C$ (highly positive mean value ranges from −23.30‰ to −33.48‰) and forest soil had the lowest (highly negative mean values range from −24.9‰ to −35.62‰). These trends are inconsistent with the bulk C $\delta^{13}C$ measurements, in particular, the bean soil signature is relatively low (more negative).

According to the main land use types, surface soil samples were grouped into 4 erosion sources: M (maize farmland), B (bean farmland), V (vegetable farmland) and F (forest). To check for significant differences of $\delta^{13}C$ values of bulk C and $\delta^{13}C_{FA}$ between soils from all investigated source plots, we applied the Kruskal-Wallis test (Table 2) to compare the isotopic signatures of distinct land use pairs, using the analytical data presented in Table 1. For $\delta^{13}C$ values of bulk soils, significant differences ($P < 0.0001$) were found for 5 out of 6 possible land use pairs, respectively. Based on $\delta^{13}C_{FA}$ values and their discriminant ability of occurrence in sediments, the suitable FAs were selected to identify land use sources. The 44 out of 54 pairwise land use comparisons revealed a difference in their $\delta^{13}C$ signature for individual FAs ($P < 0.01$) (Table 2). As expected, the majority of FAs showed a clear distinction between the $\delta^{13}C$ signatures of C_3 and C_4 plants. Greatest distinction was found for M vs. F and V vs. F (C14:0, C16:0, C18:0, C20:0, C22:0, C24:0, C26:0, C28:0, C30:0 ($P < 0.0001$)). A good separation was also found between $\delta^{13}C$ signatures of FAs for some land use pairs with only C_4 plants (e. g. M vs. B, M vs. V: C20:0, C22:0, C24:0, C26:0, C28:0, C30:0 ($P < 0.01$); B vs. V: C16:0, C20:0, C22:0, C24:0, C26:0 ($P < 0.01$)). No discrimination between C14:0 signatures of FAs were found for M vs. B and B vs. V; C18:0 signatures of FAs were found for M vs. B, M vs. V and B vs. V. Based on these results and their frequency of occurrence, bulk C-13, C16:0, C20:0, C22:0, C24:0, C26:0 and C28:0 was used for further processing.

In addition, the PCA analysis showed it accounted for 72.4% of the variance in the data for the Jiangou catchment (Fig. S2). Multiple samples collected from the same source type are generally clustered together. The $\delta^{13}C_{FA}$ values of forest, bean farmland, maize farmland and vegetable farmland formed the four clusters which was indicated that the sources discrimination in different principal component and the distribution of the different isotopic signatures of the fatty acids for the sources. The analysis validated our above selection of the best suitable biomarkers.

Then the fatty acid selection was carried out by evaluating the validity of the point-in-polygon criterion based on the principle

Table 1
Summary of the mean % C and $\delta^{13}C$ values of bulk C and $\delta^{13}C_{FA}$ for each soil source in the study catchment.

Land uses	Maize farmland		Bean farmland		Vegetable farmland		Forest land		Sediment	
	Mean	SD	Mean	SD	Mean	SD	Mean	SD	Mean	SD
	n = 9		n = 7		n = 8		n = 11		n = 7	
C%	0.65	0.09	1.14	0.09	1.24	0.15	1.59	0.31	0.94	0.06
Bulk $\delta^{13}C$	−20.58	0.25	−24.78	0.32	−21.53	0.50	−23.98	0.24	−21.89	0.30
C14:0	−24.74	0.39	−25.27	0.46	−25.44	0.44	−27.09	0.19	−26.89	0.24
C16:0	−24.21	0.28	−25.56	0.36	−24.32	0.46	−27.41	0.37	−28.06	0.54
C18:0	−23.30	0.33	−23.46	0.35	−23.39	0.49	−24.90	1.04	−25.11	0.28
C20:0	−29.16	0.91	−27.65	0.43	−23.81	1.15	−31.59	0.44	−28.18	0.56
C22:0	−30.77	0.44	−31.98	0.45	−24.67	0.54	−31.68	0.45	−30.19	0.28
C24:0	−30.38	0.45	−33.63	0.28	−24.46	0.45	−34.20	0.95	−30.76	0.28
C26:0	−30.17	0.42	−31.76	0.25	−29.49	0.48	−35.62	0.41	−30.54	0.50
C28:0	−32.17	0.29	−33.42	0.24	−33.24	1.15	−35.49	1.17	−31.94	0.58
C30:0	−32.35	0.36	−33.48	0.22	−33.24	0.54	−34.04	0.52	−33.98	0.70

Table 2
Significance levels derived from an Kruskal-Wallis Test of $\delta^{13}C$ values of bulk carbon and different FAs for pairwise combinations of land use soil samples.

Land use pairs	Bulk ^{13}C	C14:0	C16:0	C18:0	C20:0	C22:0	C24:0	C26:0	C28:0	C30:0
M-B	**	n.s.	**	n.s.	**	**	**	**	**	**
M-V	**	**	n.s.	n.s.	**	**	**	*	n.s.	**
M-F	****	****	****	****	****	**	****	****	****	**
B–V	**	n.s.	**	n.s.	**	**	**	**	n.s.	n.s.
B–F	**	****	****	**	****	n.s.	n.s.	****	****	*
V–F	****	****	****	**	****	****	****	****	**	*

Abbreviations: Maize (M), Bean (B), Vegetable (V), Forest (F).
Significance codes: non-significant ($p > 0.05$) 'ns'; $p < 0.05$ '*'; $p < 0.01$ '**'; $p < 0.001$ '***'; $p < 0.0001$ '****'.

that the $\delta^{13}C_{FA}$ values of the mixture should fall within the mixing polygon of $\delta^{13}C_{FA}$ isotopic value (s) of all sources (Phillips & Gregg, 2003; Phillips et al., 2014). Fig. S3 showed that only bulk $\delta^{13}C$, C20:0, C22:0, C24:0 and C26:0 were selected which satisfied these key criteria, proving their conservativeness in this study.

3.2. Variation of ^{137}Cs and $^{210}Pbex$ source signatures

The activity of ^{137}Cs and $^{210}Pbex$ for different sources and sediment in the Jiangou catchment was presented by Fig. 2. As expected, hillslope surface soils (maize, bean, vegetable and forest) showed higher ^{137}Cs (averaged 1.47 ± 0.54 Bq kg^{-1}) and $^{210}Pbex$ (averaged 18.68 ± 5.08 Bq kg^{-1}) concentrations than sub-surface source (channel bank) of averaged 0.26 ± 0.02 Bq kg^{-1} for ^{137}Cs and 10.17 ± 0.25 Bq kg^{-1} for $^{210}Pbex$. This implies that these two tracers can discriminate the surface soil sources from sub-surface soil. The results further showed that among the hillslope surface soil sources, ^{137}Cs and $^{210}Pbex$ are generally higher in forest soil compared to maize, bean and vegetable soils. Forestland had the most enriched ^{137}Cs concentration ranging from 1.78 to 2.30 Bq kg^{-1}, and $^{210}Pbex$ concentration ranging from 23.50 to 32.12 Bq kg^{-1}. Maize farmland exhibited the lowest ^{137}Cs and $^{210}Pbex$ values, in a range of 0.65–1.03 Bq kg^{-1} and 13.24–16.09 Bq kg^{-1}. ^{137}Cs and $^{210}Pbex$ of sediment were between the values of hillslope surface soil sources and channel banks.

3.3. Apportionment of sediment sources by FRNs-CSSI fingerprinting

The FRNs-based fingerprinting was employed to determine the relative contributions of surface (i.e. hillslope surface soils) and sub-surface (i.e. channel bank) sediment sources to the sediment deposit (Fig. 5). The results indicated that surface and sub-surface soils accounted for 62 ± 7% and 38 ± 7% to the sediment in Jiangou catchment. The proportions of different land use types on hillslopes in sediment from the outlet of the catchment were conducted by CSSI-based fingerprinting and calculated using the MixSIAR model. The values of $\delta^{13}C$ signatures of the selected long-chain FAs (C20:0, C22:0, C24:0, C26:0 and C28:0) and bulk $\delta^{13}C$ of the land use-based source soils and sediment performed best when running MixSIAR model. Matrix plots of estimates of each source isotopic proportion displayed correlation values between sources (Fig. 3). Well-separated sources are characterized by weak correlation values (e.g. −0.11 forest vs. maize, 0.17 forest vs. vegetable). Sources close to each other resulted in strong correlations (e.g. −0.76 maize vs. vegetable, −0.71 bean vs. forest). Increased correlation among sources will increase the level of uncertainty in the model output of estimates of each source proportion displayed correlation values between sources (Fig. 3). The correction based on the %C org. of each source was used to convert the resulting isotopic proportions into soil proportions (Fig. 4). Our soil proportion results suggest that the sources of maize, bean, vegetable and forest soils contributed 71 ± 6%, 16 ± 2%, 10 ± 1% and 3 ± 2% respectively, to the sediment at the outlet of catchment.

To obtain more accurate and effective sediment sources, the novel combination of FRNs and CSSI fingerprinting was employed to all sediment sources apportionment in the catchment (Fig. 4). The dominant sediment source was derived from maize farmland which contributed 44 ± 0.1%, followed by channel bank (38 ± 7%), bean farmland (10 ± 0.2%) and vegetable farmland (6 ± 0.2%), and least by forestland (2 ± 0.8%). It is noted that the contribution of the sub-surface source (i.e. channel bank) to sediment in the deposition zone was comparable to that of maize. This was further corroborated as the channel bank covered less area than maize fields but made a significant sediment contribution (Fig. 5).

3.4. Reference value of ^{137}Cs and sedimentation rate

A composite sample was used to determine the profile distribution of the ^{137}Cs reference site and its maximum depth. The

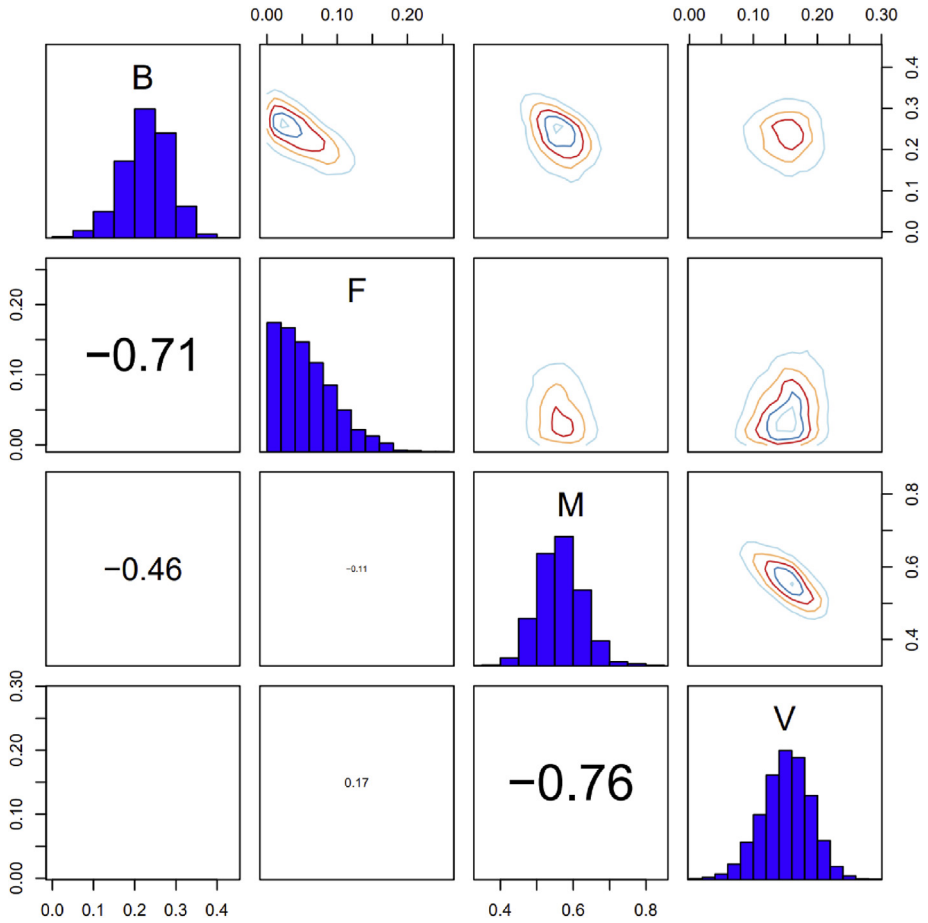

Fig. 3. Matrix plot of estimates of each source isotopic proportion calculated in the mixing models from the MixSIAR package output, represented by simulated values of the isotopic proportions in the histograms. Correlation values between sources are inside the boxes to the left of histograms.

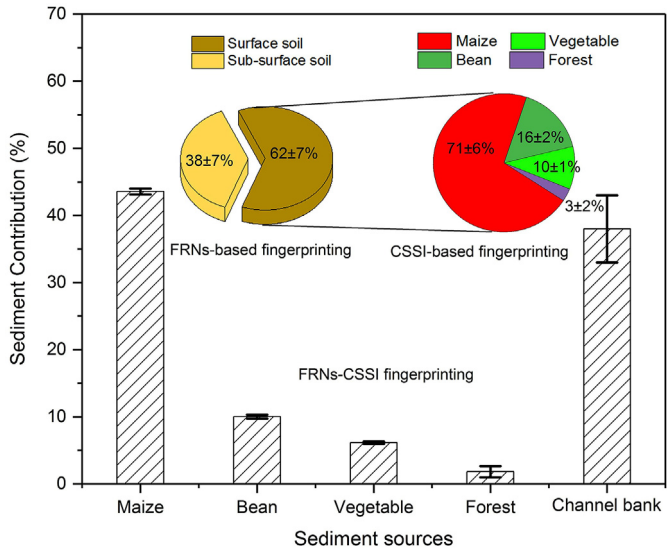

Fig. 4. Contribution of different sediment sources to the sediment production in this catchment by FRN-based sediment fingerprinting, CSSI-based sediment fingerprinting and combined FRNs and CSSI fingerprinting techniques.

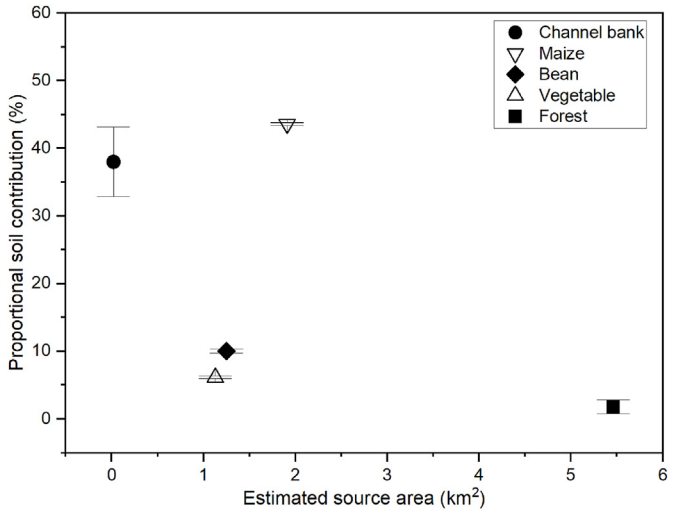

Fig. 5. Scatter plot showing the comparison between proportional soil contributions (%) of the investigated sediment sources and the estimated corresponding land areas (km^2) covered by the different land uses and channel banks. Land uses are summarized as maize, bean, vegetable and forest.

concentration of ^{137}Cs in the 0–5 cm soil layers was 5.90 Bq kg^{-1}, and decreased exponentially to 0.33 Bq kg^{-1} in the 25–30 cm depth. No ^{137}Cs was detected below the 30 cm layer. Fig. 6 shows the vertical distribution of the ^{137}Cs inventory in the reference site using the composite sample. 94% of the ^{137}Cs is accumulated in the upper 20 cm and the results show an exponential decrease of the

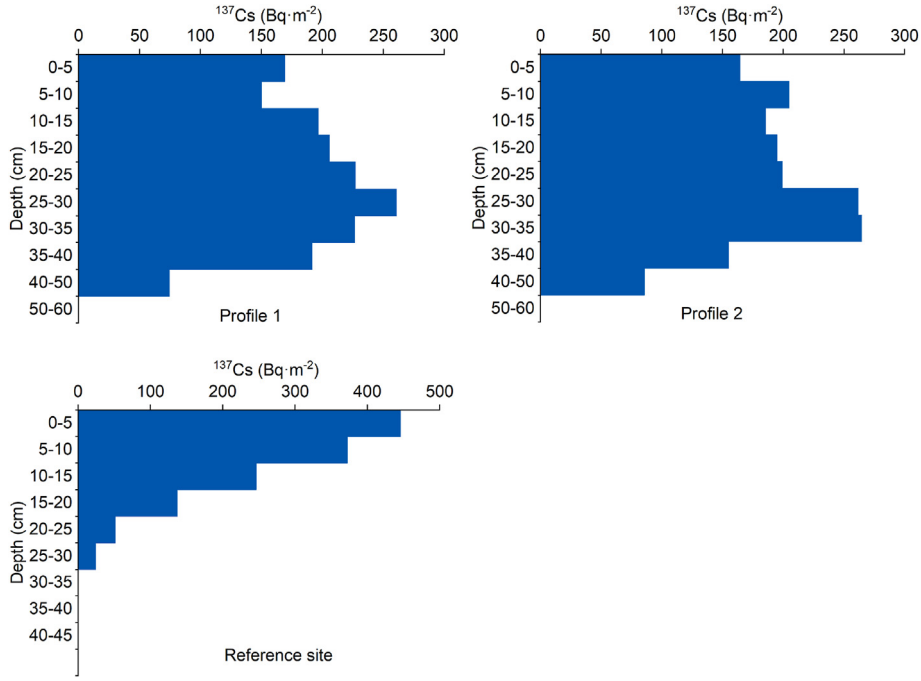

Fig. 6. The area activity of ^{137}Cs of reference site, profile 1 and profile 2 at the outlet of Jiangou catchment.

^{137}Cs areal activity with depth for a total activity profile of 1276 Bq m^{-2}. The ^{137}Cs inventory for the 5 grassland samples ranged from 943.11 to 1534.36 Bq m^{-2} with the CV of 17.22%.

The ^{137}Cs inventory of the profile 1 and profile 2 were 1701.76 and 1715.66 Bq m^{-2} with the maximum activities of 3.54 and 3.44 Bq kg^{-1}, respectively in the 25–30 cm soil layer. ^{137}Cs was present to the 50 cm depth. The maximum areal activities were found at 25–30 and 30–35 cm depth with respective values of 260.76 and 264.51 Bq m^{-2} for profile 1 and profile 2, respectively (Fig. 6). The ^{137}Cs distribution indicates quite well the sedimentation process in the deposition area with an ^{137}Cs inventory significantly higher than the reference site. The sedimentation rates for two profiles were estimated using MBM 2. The mean and standard deviation of sedimentation rate was 13.55 ± 0.3 t ha^{-1} yr^{-1}.

3.5. Total N and total P loads from different sediment sources

The averaged sedimentation rate combined with the area of different sediment sources and sediment source apportionment, were used to estimate the annual output of total N and total P loadings in sediment from different sediment sources in Jiangou catchment. The results suggested that the total N loss was the largest in maize farmland (0.98 ± 0.12 t yr^{-1}), followed by bean farmland (0.21 ± 0.02 t yr^{-1}), forest land (0.20 ± 0.02 t yr^{-1}) and vegetable farmland (0.14 ± 0.01 t yr^{-1}), and the contribution of channel bank (0.01 ± 0.001 t yr^{-1}) was the least. The same trend was found in total P loss from different sediment sources, but the magnitude of total P (1.86 ± 0.09 t yr^{-1}) derived from maize farmland was much higher than total N (Fig. 7).

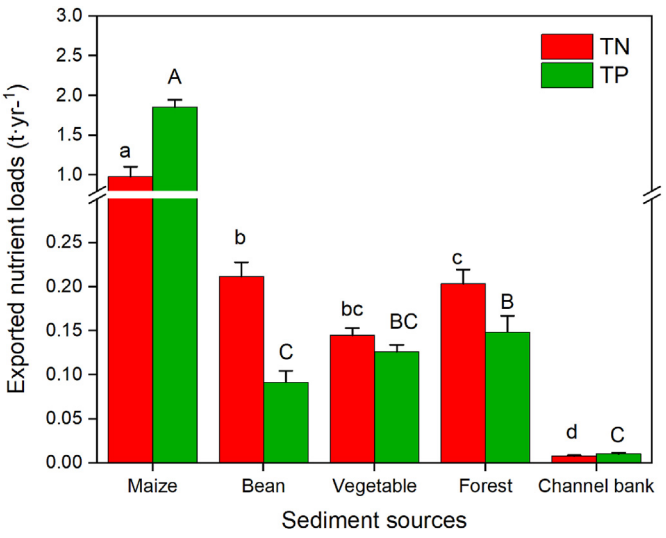

Fig. 7. Magnitude of total nitrogen (TN) and total phosphorus (TP) in sediment exported from different sediment sources in Jiangou catchment. Lowercase letters represent the difference of TN load from different sediment sources and uppercase letters represent the difference of TP. Different letters indicate significant differences ($P < 0.05$).

4. Discussion

4.1. $\delta^{13}C_{FA}$, bulk$\delta^{13}C$ and FRNs signatures for sediment source discrimination

The $\delta^{13}C_{FA}$ values for maize, bean and vegetable farmlands (more positive, C4 plant) are well discriminated from the $\delta^{13}C_{FA}$ value of forest soil (more negative, C3 plant) (Hirave et al., 2020; Mabit et al., 2018), but these trends are inconsistent with the bulk C $\delta^{13}C$ measurements, in particular, the bean soil signature is relatively more negative (Table 1). It is implying that bulk organic matter within the soil is dominated by the forest signal (C3-derived material) and not the bean crop itself. These results are supported by previous works revealing that the bulk $\delta^{13}C$ signatures were heavily influenced by past crop rotation or other C sources used in source tracer studies (Blake et al., 2012; Mabit et al., 2018; Upadhayay et al., 2017).

The statistical analysis and polygon test were used to determine

which FAs were best suited to discriminate between the sources. Bulk $\delta^{13}C$ and $\delta^{13}C_{FA}$ of C20:0, C22:0, C24:0 and C26:0 were selected which satisfied these key criteria to allow the best discrimination in this study. These results support the conclusion of previous field studies of the usefulness of saturated long-chain FAs (Alewell et al., 2016; Gibbs et al., 2020; Hirave et al., 2020; Mabit et al., 2018), as the long-chain saturated FAs mostly produced by vascular plants are more reliable fingerprints than short-chain FAs (Upadhayay et al., 2017).

In addition, the topsoil of ^{137}Cs and $^{210}Pbex$ were used to discriminate the sediment source from surface and sub-surface erosion sources. The hillslope surface soils from maize, bean and vegetable farmlands and forestland showed higher concentrations of ^{137}Cs and $^{210}Pbex$ than those in sub-surface soil from channel bank, which suggests that these two tracers can discriminate the surface and sub-surface erosion sources (Fig. 2). Similar results are seen in the Mitchell and Logan catchments in eastern Australia (Hancock et al., 2014), two major northern Australian Rivers (Caitcheon et al., 2012) and in northern part of the New Zealand (Hughes et al., 2021). Given that long-term rainfall and local sedimentation rates are generally higher in forests, forest soil concentrations are therefore higher. Sub-surface soil samples from channel banks showed low concentrations of ^{137}Cs and $^{210}Pbex$ reflecting the very low surface soil component associated with these sources.

4.2. Source sediment contributions using FRNs-CSSI fingerprinting

To obtain accurate and effective sediment sources, we used FRNs-based fingerprinting to distinguish the contribution of surface (i.e., hillslope surface soils) and sub-surface (i.e., channel bank) erosion materials to sediment in catchment landscapes, while using the combination of CSSI-based fingerprinting to identify the proportions of different land use types in source surface soil in the sediment. This approach enabled all of the sediment sources to be apportioned (Fig. 4). The vegetation-specific tracers used in CSSI-based fingerprinting are mostly accumulated in the surface soils from above-ground biomass deposition and root input (Hirave et al., 2020). Also, the vertical transport of these tracers in soils, especially the $\delta^{13}C$ of long chain fatty acids across sub-soil horizons, is limited and tracer content from deeper sub-soil horizons may not be usually sufficient for reliable sediment source apportionment (Jansen & Wiesenberg, 2017). Hence, one of the limitations of the CSSI-based fingerprinting is its inability to distinguish between surface and sub-surface erosion such as gully and streambank erosion (Hirave et al., 2020). Therefore, it is necessary for CSSI-based fingerprinting to be combined with FRNs that can distinguish between surface and sub-surface erosion sources in geomorphologically active landscapes. Recent research in a Mediterranean agroforestry catchment demonstrated that the CSSI complement improved the detection of channel bank and subsoil with tracers such as radionuclides and stable elements to give a complete picture of the sources supplying sediments in severely dissected landscapes (Lizaga et al., 2021).

Our results indicated that the contributions of surface (hillslope surface soils) and sub-surface (channel bank) soils to the sediment in Jiangou catchment were discriminated by using FRNs-based fingerprinting. There have also been some previous reports using FRNs to successfully discriminate the source of surface and sub-surface soil to the sediment mixture (Hancock et al., 2014; Hughes et al., 2021; Olley et al., 2013). The source apportionment of different land use types (maize, bean, vegetable and forest) in hillslope surface soil to the sediment at the outlet of the catchment were also identified by CSSI-based fingerprinting. The contribution of the sources to the sediment is in accordance with their geomorphological and temporal vegetation-specific characteristics. Maize farmland had the highest sediment contribution because maize is considered one of the most erosive crops, especially at the beginning of the growing season and harvesting season, when the soil is tillage, roots are dug out and soil is left bare or exposed to water erosion for long periods of time throughout the entire year (Brandt et al., 2016; Mabit et al., 2018; Tuan et al., 2014). In addition, parts of maize fields were very close to the outlet of the main stream of the catchment so their sediment connectivity is high (Koci et al., 2019) (Fig. 1b), which could further support the washing of soil particles by water erosion. Conversely, bean and vegetable fields are relatively less disturbed, so soil erosion and washing away of sediment are also relatively low. With regard to forest, multi-stories and overlapping vegetation covers, these vertical structures reduce soil erosion by reducing raindrop strikes and increasing infiltration resulting in the lowest runoff with minimum sediment movement and contribution to sediment sources (Sun et al., 2018).

All sediment sources apportionment in Jiangou catchment were conducted by the novel combination of FRNs and CSSI fingerprinting. The contribution of sub-surface source (i.e. channel bank) to sediment in the deposition zone was comparable to that of maize. Similar observation was reported by many scientists. For instance, Hughes et al. (2021) found that the stream bank can contribute very high proportions of sediment within New Zealand catchments; Shi et al. (2021) identified the incised and actively eroding channel banks were the most important source of sediment (over 80%), in a small catchment in the Upper Yangtze River basin of China. The comparison between proportional soil contributions (%) of the investigated sediment sources and the corresponding source areas (km^2) is shown in Fig. 5. The ratio of sediment contribution to source area decreased as following order: channel bank (18.3) > maize (0.24) > bean (0.08) > vegetable (0.05) > forest (0.003). These results revealed that the sub-surface sources deliver a disproportionately large percentage of annual sediment loads to water bodies when compared to forest lands, and crops (maize, bean and vegetable) farmlands representing more erosion-prone land use types than forests. In addition, these trends were also closely related to sediment connectivity. The forest had lower IC values, mainly because of the higher vegetation cover, and the soil fixation of the root system is not only influencing its erosion index but also has the function of sediment interception, so the forest contributed less to sediment. This result is consistent with the study of Yan et al. (2022), which showed that land use types with vegetation cover had lower IC values than land without vegetation cover. Koci et al. (2019) found that sediment connectivity across all hillslopes is generally the highest closest to the main channel and progressively decreases away from it. This supports our finding that the channel bank has the highest sediment connectivity, followed by maize, bean and vegetable farmlands. In this study, the effects of slope (Zhang et al., 2019) and land use patches (Fang, 2020) on sediment connectivity were similar in all sources due to our catchment characteristics, so the differences in the impact of slope and land use patches on IC in different sediment sources were negligible.

4.3. Quantification of sediment total N and total P outputs from different sediment sources and implications

The magnitude of total N and total P derived from different sediment sources in Jiangou catchment was quantitatively estimated by the combined use of FRN and CSSI techniques. In this study, ^{137}Cs-derived sedimentation rate (13.55 ± 0.3 t ha^{-1} yr^{-1}) at the outlet of the catchment was analyzed with the reference value of 1276 Bq m^{-2} and two cores collected in a depositional area.

Previous studies proposed a reference value in 2002 (1923 Bq m^{-2}) for the Luanhe River source area, Fengning County near the northern suburban region of Beijing (Zhao et al., 2005). This effective ^{137}Cs reference value decayed to 1301 Bq m^{-2} by 2019. A study on the ^{137}Cs reference values in China used the Modified CRI (Cs-137 Reference Inventory) Model for the Mainland of China (MCM) model with high accuracy compared with ^{137}Cs reference value measurements. This study proposed reference value of ^{137}Cs near Beijing in 2015 was 1560 Bq m^{-2} (Wei et al., 2015). The effective ^{137}Cs inventory in 2019 decayed to an estimated 1423 Bq m^{-2}. Therefore, the ^{137}Cs reference value in our study is deemed acceptable and within the range of results reported on the above reference sites.

Combining the sedimentation rate with the area of different sediment sources and sediment source apportionment by FRN and CSSI fingerprinting, we quantified that the total N and total P in sediment were both dominantly derived from maize farmland (0.98 ± 0.12 and 1.86 ± 0.09 t yr^{-1}), and the least came from channel bank (0.01 ± 0.001 and 0.01 ± 0.001 t yr^{-1}), but the magnitude of total P derived from maize farmland was much higher than that of total N (Fig. 7). The previous studies have supported our findings. By comparing soil erosion and its effects on soil nutrients under different land use types (forestland, abandoned land, arable land and grassland) in the Shuanglongliu Area of Dianchi Lake, researchers found that the greatest loss of nutrients is due to erosion during tillage in the cultivated farmland (Niu et al., 2015). The study of erosion on small watershed in hilly and gully region of Loess Plateau revealed that the TN and TP in farmland soil decreased in the last 18 years. The loss of TP was significantly greater than that of TN (Porto & Callegari, 2021; Wu et al., 2016), which may be because under the same environmental conditions, the solubility of N is higher than that of P, and the uptake of nitrogen by crop roots was greater than that of P.

It is interesting to note that the contribution of the channel banks to sediment is comparable to that of maize farmlands, but the contribution to nitrogen and phosphorus nutrients that affect eutrophication of water body is quite small. Granger et al. (2021) also found that the slightly lower TP concentrations measured at exposed channel bank samples indicated that banks that are actually eroding may be contributing less TP than the total channel bank TP values measured across the catchments as a whole, which attribute to an increased contribution of subsoil from actively eroding taller channel banks. Similarly, the contribution of channel bank to the nitrogen load in sediment is also quite low, this is mainly due to the lower TN content in the channel bank subsurface soil after erosion (Yang et al., 2018). This implies that managers should place equal emphasis on reducing pollution (increasing fertilizer efficiency) and reducing soil erosion on chemical-applied farmlands (maize farmlands) in this catchment. As for the sub-surface soil erosion, like the channel bank, it is mainly to prevent its erosion collapse.

5. Conclusion

The novel application of CSSI and FRNs (^{137}Cs and ^{210}Pbex) tracer approaches demonstrated here offers an important new tool to quantify sediment sources and associated total N and total P loads in an intensive agricultural catchment. The FRNs-based fingerprinting identified that sediment sources from surface soils (i.e. hillslope surface soils) were almost double that of sub-surface soils (i.e. channel banks) within the catchment. The δ^{13}C signatures of particle-associated fatty acids are able to differentiate sediment sources linking to the fields under specific vegetation cover in hillslopes. The novel combination of FRNs and CSSI fingerprinting techniques provided unique insights into quantitatively identifying sediment source and associated total N and total P in the context of signature development processes. Our study identified maize farmland as the dominant sediment source followed by channel bank, bean farmland, vegetable farmland and least by forest land in this catchment. Combining with ^{137}Cs-derived sedimentation rate at the outlet of the catchment, the total N and total P loads in the sediment exported from different sediment sources were quantified. Channel banks cause comparable sediment input with maize farmlands, but the contribution to N and P nutrients that affect the eutrophication of water bodies is quite small. Our study suggested the chemical-applied farmlands are still the main hotspots of catchment non-point source pollution prevention and control, which should place equal emphasis on reducing pollution (increasing fertilizer efficiency) and reducing soil erosion at the same time. While for the sub-surface soil erosion, like channel bank, preventing erosion collapse is the focus of this catchment. The novel conjunctive use of FRNs and CSSI techniques can cost-effectively quantify the sediment N and P loads from different sediment sources, especially in the first-visiting catchment, which are critical to the assessment and implementation of optimized agricultural and land management practices.

Declaration of competing interest

The authors declare that they have no known competing financial interests or personal relationships that could have appeared to influence the work reported in this paper.

Acknowledgments

This work was supported by the International Atomic Energy Agency through coordination research projects (CRP) under Research Contract No. 23008 and technical cooperation project (TCP) RAS 5084, and the Central Public-interest Scientific Institution Basal Research Fund (No. BSRF202004). Funding for AC to collaborate on this work was provided by the High-end Foreign Experts Recruitment Program from State of Administration of Foreign Experts Affairs of China. This work was partly supported by the Science and Technology Major Project of Guangxi (Guike AA17204078).

Appendix A. Supplementary data

Supplementary data to this article can be found online at https://doi.org/10.1016/j.iswcr.2022.10.006.

References

Alewell, C., Birkholz, A., Meusburger, K., Schindler Wildhaber, Y., & Mabit, L. (2016). Quantitative sediment source attribution with compound-specific isotope analysis in a C3 plant-dominated catchment (central Switzerland). *Biogeosciences, 13*(5), 1587–1596.

Astakhov, A. S., Sattarova, V. V., Xuefa, S., Limin, H., Aksentov, K. I., Alatortsev, A. V., … Mariash, A. A. (2019). Distribution and sources of rare earth elements in sediments of the Chukchi and East Siberian Seas. *Polar. Sci., 20*, 148–159.

Bai, Y., Zha, X., Zhang, J., & Chen, S. (2020). The threshold of nitrogen and phosphorus loss in runoff on degraded Ferralsols of Fujian province, southern China. *Environmental Earth Sciences, 79*(16).

Blake, W. H., Ficken, K. J., Taylor, P., Russell, M. A., & Walling, D. E. (2012). Tracing crop-specific sediment sources in agricultural catchments. *Geomorphology, 139–140*, 322–329.

Borselli, L., Cassi, P., & Torri, D. (2008). Prolegomena to sediment and flow connectivity in the landscape: A gis and field numerical assessment. *Catena, 75*(3), 268–277.

Brandt, C., Cadisch, G., Nguyen, L. T., Vien, T. D., & Rasche, F. (2016). Compound-specific δ^{13}C isotopes and Bayesian inference for erosion estimates under different land use in Vietnam. *Geoderma Regional, 7*(3), 311–322.

Bravo-Linares, C., Schuller, P., Castillo, A., Ovando-Fuentealba, L., Munoz-Arcos, E., Alarcon, O., … Dercon, G. (2018). First use of a compound-specific stable isotope (CSSI) technique to trace sediment transport in upland forest catchments of

Chile. *Science of the Total Environment, 618*, 1114–1124.
Bremner, J. M. (1960). Determination of nitrogen in soil by the Kjeldahl method. *Journal of Agricultural Science, 55*(1), 11–33.
Brito, P., Prego, R., Mil-Homens, M., Cacador, I., & Caetano, M. (2018). Sources and distribution of yttrium and rare earth elements in surface sediments from Tagus estuary, Portugal. *Science of the Total Environment, 621*, 317–325.
Caitcheon, G. G., Olley, J. M., Pantus, F., Hancock, G., & Leslie, C. (2012). The dominant erosion processes supplying fine sediment to three major rivers in tropical Australia, the Daly (NT), Mitchell (Qld) and Flinders (Qld) Rivers. *Geomorphology, 151–152*, 188–195.
Cavalli, M., Trevisani, S., Comiti, F., & Marchi, L. (2013). Geomorphometric assessment of spatial sediment connectivity in small Alpine catchments. *Geomorphology, 188*, 31–41.
Collins, A. L., Blackwell, M., Boeckx, P., Chivers, C.-A., Emelko, M., Evrard, O., … Zhang, Y. (2020). Sediment source fingerprinting: Benchmarking recent outputs, remaining challenges and emerging themes. *Journal of Soils and Sediments, 20*, 4160–4193.
Collins, A. L., Pulley, S., Foster, I. D. L., Gellis, A., Porto, P., & Horowitz, A. J. (2017). Sediment source fingerprinting as an aid to catchment management: A review of the current state of knowledge and a methodological decision-tree for end-users. *Journal of Environmental Management, 194*, 86–108.
Evrard, O., Laceby, J. P., Ficetola, G. F., Gielly, L., Huon, S., Lefevre, I., … Poulenard, J. (2019). Environmental DNA provides information on sediment sources: A study in catchments affected by fukushima radioactive fallout. *Science of the Total Environment, 665*, 873–881.
Fang, H. (2020). Impact of land use changes on catchment soil erosion and sediment yield in the northeastern China: A panel data model application. *International Journal of Sediment Research, 35*(5), 540–549.
García-Comendador, J., Martínez-Carreras, N., Fortesa, J., Borràs, A., Calsamiglia, A., & Estrany, J. (2020). Analysis of post-fire suspended sediment sources by using colour parameters. *Geoderma, 379*.
Gholami, H., Jafari TakhtiNajad, E., Collins, A. L., & Fathabadi, A. (2019). Monte Carlo fingerprinting of the terrestrial sources of different particle size fractions of coastal sediment deposits using geochemical tracers: Some lessons for the user community. *Environmental Science and Pollution Research International, 26*(13), 13560–13579.
Gibbs, M. M. (2008). Identifying source soils in contemporary estuarine sediments: A new compound-specific isotope method. *Estuaries and Coasts, 31*(2), 344–359.
Gibbs, M. M. (2014). *Protocols on the use of compound-specific stable isotopes to identify and apportion soil sources from land use. Revised 2013. Contract report to joint FAO/IAEA division of nuclear techniques in food and agriculture*.
Gibbs, M., Leduc, D., Nodder, S. D., Kingston, A., Swales, A., Rowden, A. A., … Graham, B. (2020). Novel application of a compound-specific stable isotope (CSSI) tracking technique demonstrates connectivity between terrestrial and deep-sea ecosystems via submarine canyons. *Frontiers in Marine Science, 7*.
Granger, S. J., Harris, P., Upadhayay, H. R., Sint, H., Pulley, S., Stone, M., … Collins, A. L. (2021). Novel approaches to investigating spatial variability in channel bank total phosphorus at the catchment scale. *Catena, 202*.
Haddadchi, A., Ryder, D. S., Evrard, O., & Olley, J. (2013). Sediment fingerprinting in fluvial systems: Review of tracers, sediment sources and mixing models. *International Journal of Sediment Research, 28*(4), 560–578.
Hancock, G. J., & Revill, A. T. (2013). Erosion source discrimination in a rural Australian catchment using compound-specific isotope analysis (CSIA). *Hydrological Processes, 27*(6), 923–932.
Hancock, G. J., Wilkinson, S. N., Hawdon, A. A., & Keen, R. J. (2014). *Use of fallout tracers ^{7}Be, ^{210}Pb and ^{137}Cs to distinguish the form of sub-surface soil erosion delivering sediment to rivers in large catchments*.
Hirave, P., Glendell, M., Birkholz, A., & Alewell, C. (2020). *Compound-specific isotope analysis with nested sampling approach detects spatial and temporal variability in the sources of suspended sediments in a Scottish mesoscale catchment*. Science of The Total Environment.
Huang, D., Pei, M., Zhou, L., Fan, H., & Jia, Y. (2020). Identification of sediment sources and exploration of scale effects in the black soil region of Northeast China. *Catena, 195*.
Hughes, A. O., Huirama, M. K., Owens, P. N., & Petticrew, E. L. (2021). Stream bank erosion as a source of sediment within New Zealand catchments. *New Zealand Journal of Marine & Freshwater Research*, 1–24.
Hu, J., Zhang, H., & Peng, P.a. (2006). Fatty acid composition of surface sediments in the subtropical Pearl River estuary and adjacent shelf, Southern China. *Estuarine, Coastal and Shelf Science, 66*(1–2), 346–356.
IAEA. (2019). Guidelines for sediment tracing using the compound-specific carbon stable isotope technique. *IAEAL, 19–01260*, 978–92–0–158519–6 (paperback : alk. paper), Vienna.
Jansen, B., & Wiesenberg, G. L. B. (2017). Opportunities and limitations related to the application of plant-derived lipid molecular proxies in soil science. *Soil., 3*, 211–234.
Kobe, F., Leipe, C., Shchetnikov, A. A., Hoelzmann, P., Gliwa, J., Olschewski, P., … Tarasov, P. E. (2021). Not herbs and forbs alone: Pollen-based evidence for the presence of boreal trees and shrubs in cis-baikal (eastern siberia) derived from the last glacial maximum sediment of lake ochaul. *Journal of Quaternary Science*, 1–16.
Koci, J., Sidle, R. C., Jarihani, B., & Cashman, M. J. (2019). Linking hydrological connectivity to gully erosion in savanna rangelands tributary to the Great Barrier Reef using structure-from-motion photogrammetry. *Land Degradation & Development, 31*(1), 20–36.
Li, Y., Gholami, H., Song, Y., Fathabadi, A., Malakooti, H., & Collins, A. L. (2020). Source fingerprinting loess deposits in Central Asia using elemental geochemistry with Bayesian and GLUE models. *Catena, 194*.
Li, Y., Poesen, J., Yang, J. C., Fu, B., & Zhang, J. H. (2003). Evaluating gully erosion using ^{137}Cs and ^{210}Pb/^{137}Cs ratio in a reservoir catchment. *Soil and Tillage Research, 69*(1–2), 107–115.
Li, T., Sun, G., Yang, C., Liang, K., Ma, S., Huang, L., & Luo, W. (2019). Source apportionment and source-to-sink transport of major and trace elements in coastal sediments: Combining positive matrix factorization and sediment trend analysis. *Science of the Total Environment, 651*(Pt 1), 344–356.
Li, H., Wang, Y., Shi, L. Q., Mi, J., Song, D., & Pan, X. J. (2012). Distribution and fractions of phosphorus and nitrogen in surface sediments from Dianchi Lake, China. *International Journal of Environmental Research, 6*(1), 1735–6865.
Lizaga, I., Bode, S., Gaspar, L., Latorre, B., Boeckx, P., & Navas, A. (2021). Legacy of historic land cover changes on sediment provenance tracked with isotopic tracers in a Mediterranean agroforestry catchment. *Journal of Environmental Management, 288*, Article 112291.
Li, X., Zhao, Y., Wang, G., Han, R., Dang, X., Li, Z., … Gao, C. (2020). Sedimentary nitrogen fractions and source assignment from different inflows to a receiving lake. *Water Supply, 20*(5), 1950–1964.
Mabit, L., Gibbs, M., Mbaye, M., Meusburger, K., Toloza, A., Resch, C., … Alewell, C. (2018). Novel application of Compound Specific Stable Isotope (CSSI) techniques to investigate on-site sediment origins across arable fields. *Geoderma, 316*, 19–26.
Mabit, L., Klik, A., Benmansour, M., Toloza, A., Geisler, A., & Gerstmann, U. C. (2009). Assessment of erosion and deposition rates within an Austrian agricultural watershed by combining 137Cs, 210Pbex and conventional measurements. *Geoderma, 150*(3–4), 231–239.
Mendoza-Fernández, A. J., Peña-Fernández, A., Molina, L., & Aguilera, P. A. (2021). The role of technology in greenhouse agriculture: Towards a sustainable intensification in campo de Dalías (Almería, Spain). *Agronomy, 11*(1).
Niu, X.-Y., Wang, Y.-H., Yang, H., Zheng, J.-W., Zou, J., Xu, M.-N., … Xie, B. (2015). Effect of land use on soil erosion and nutrients in Dianchi Lake watershed, China. *Pedosphere, 25*(1), 103–111.
Ni, Z., Wang, S., Chu, Z., & Jin, X. (2015). Historical accumulation of N and P and sources of organic matter and N in sediment in an agricultural reservoir in Northern China. *Environmental Science and Pollution Research International, 22*(13), 9951–9964.
Nosrati, K. (2017). Ascribing soil erosion of hillslope components to river sediment yield. *Journal of Environmental Management, 194*, 63–72.
Nosrati, K., Akbari-Mahdiabad, M., Fiener, P., & Collins, A. L. (2021). Using different size fractions to source fingerprint fine-grained channel bed sediment in a large drainage basin in Iran. *Catena, 200*.
Olley, J., Brooks, A., Spencer, J., Pietsch, T., & Borombovits, D. (2013). Subsoil erosion dominates the supply of fine sediment to rivers draining into Princess Charlotte Bay, Australia. *Journal of Environmental Radioactivity, 124*, 121–129.
Owens, P. N., Blake, W. H., Gaspar, L., Gateuille, D., Koiter, A. J., Lobb, D. A., … Woodward, J. C. (2016). Fingerprinting and tracing the sources of soils and sediments: Earth and ocean science, geoarchaeological, forensic, and human health applications. *Earth-Science Reviews, 162*, 1–23.
Pennock, D. J., & Appleby, P. G. (2002). Sample processing. In F. Zapata (Ed.), *Handbook for the assessment of soil erosion and sedimentation using environmental radionuclides* (pp. 111–164). Dordrecht, The Netherlands: Kluwer Ac. Publ.
Peris, A., Barbieri, M. V., Postigo, C., Rambla-Alegre, M., Lopez de Alda, M., & Eljarrat, E. (2022). Pesticides in sediments of the Ebro River Delta cultivated area (NE Spain): Occurrence and risk assessment for aquatic organisms. *Environmental Pollution, 305*, Article 119239.
Phillips, D. L., & Gregg, J. W. (2003). Source partitioning using stable isotopes: Coping with too many sources. *Oecologia, 136*(2), 261–269.
Phillips, D. L., Inger, R., Bearhop, S., Jackson, A. L., Moore, J. W., Parnell, A. C., … Ward, E. J. (2014). Best practices for use of stable isotope mixing models in food-web studies. *Canadian Journal of Zoology, 92*(10), 823–835.
Porto, P., & Callegari, G. (2021). Using Be-7 measurements to explore the performance of the SEDD model to predict sediment yield at event scale. *Catena, 196*.
Prabhakar, S. V. R. K. (2021). A succinct review and analysis of drivers and impacts of agricultural land transformations in Asia. *Land Use Policy, 102*.
Quinton, J. N., Govers, G., Van Oost, K., & Bardgett, R. D. (2010). The impact of agricultural soil erosion on biogeochemical cycling. *Nature Geoscience, 3*(5), 311–314.
Rattan, K. J., Corriveau, J. C., Brua, R. B., Culp, J. M., Yates, A. G., & Chambers, P. A. (2017). Quantifying seasonal variation in total phosphorus and nitrogen from prairie streams in the Red River Basin, Manitoba Canada. *Science of the Total Environment, 575*, 649–659.
Reiffarth, D. G., Petticrew, E. L., Owens, P. N., & Lobb, D. A. (2016). Sources of variability in fatty acid (FA) biomarkers in the application of compound-specific stable isotopes (CSSIs) to soil and sediment fingerprinting and tracing: A review. *Science of the Total Environment, 565*, 8–27.
Robotham, J., Old, G., Rameshwaran, P., Sear, D., Gasca-Tucker, D., Bishop, J., … McKnight, D. (2021). Sediment and nutrient retention in ponds on an agricultural stream: Evaluating effectiveness for diffuse pollution mitigation. *Water, 13*(12).
Selman, M., & Greenhalgh, S. (2010). Eutrophication: Sources and drivers of nutrient pollution. *Renewable Resources Journal, 26*(4), 19–26.

Shen, Y., Peng, C., Yuan, P., Wu, X., Jiang, L., Chen, S., & Song, X. (2021). Seasonal and spatial distribution and pollution assessment of nitrogen and phosphorus in sediments from one of the world's largest tidal reservoirs. *Water, 13*(4).

Sherrell, C. G., & Saunders, W. M. H. (1966). An evaluation of methods for the determination of total phosphorus in soils. *New Zealand Journal of Agricultural Research, 9*(4), 972–979.

Shi, Z., Blake, W. H., Wen, A., Chen, J., Yan, D., & Long, Y. (2021). Channel erosion dominates sediment sources in an agricultural catchment in the Upper Yangtze basin of China: Evidence from geochemical fingerprints. *Catena, 199*.

Smith, H. G., & Blake, W. H. (2014). Sediment fingerprinting in agricultural catchments: A critical re-examination of source discrimination and data corrections. *Geomorphology, 204*, 177–191.

Song, Q. (1982). *The error and data evaluation in ration analysis*. Beijing: Beijing People Education Press.

Stock, B. C., Jackson, A. L., Ward, E. J., Parnell, A. C., Phillips, D. L., & Semmens, B. X. (2018). Analyzing mixing systems using a new generation of Bayesian tracer mixing models. *PeerJ, 6*, Article e5096.

Stock, B., & Semmens, B. (2018). *MixSIAR GUI user manual*. Version 3.1.9.

Sun, D., Zhang, W., Lin, Y., Liu, Z., Shen, W., Zhou, L., … Fu, S. (2018). Soil erosion and water retention varies with plantation type and age. *Forest Ecology and Management, 422*, 1–10.

Torres Astorga, R., Garcias, Y., Borgatello, G., Velasco, H., Padilla, R., Dercon, G., & Mabit, L. (2020). Use of geochemical fingerprints to trace sediment sources in an agricultural catchment of Argentina. *International Soil and Water Conservation Research, 8*(4), 410–417.

Tuan, V. D., Hilger, T., MacDonald, L., Clemens, G., Shiraishi, E., Vien, T. D., … Cadisch, G. (2014). Mitigation potential of soil conservation in maize cropping on steep slopes. *Field Crops Research, 156*, 91–102.

Upadhayay, H. R., Bodé, S., Griepentrog, M., Huygens, D., Bajracharya, R. M., Blake, W. H., … Boeckx, P. (2017). Methodological perspectives on the application of compound-specific stable isotope fingerprinting for sediment source apportionment. *Journal of Soils and Sediments, 17*(6), 1537–1553.

Upadhayay, H. R., Smith, H. G., Griepentrog, M., Bode, S., Bajracharya, R. M., Blake, W., … Boeckx, P. (2018). Community managed forests dominate the catchment sediment cascade in the mid-hills of Nepal: A compound-specific stable isotope analysis. *Science of the Total Environment, 637–638*, 306–317.

Verma, K., Bhattacharya, S., Biswas, P., Shrivastava, P. K., Pandey, M., & Pant, N. C. (2014). Clay mineralogy of the ocean sediments from the wilkes land margin, east Antarctica: Implications on the paleoclimate, provenance and sediment dispersal pattern. *International Journal of Earth Sciences, 103*(8), 2315–2326.

Walling, D. E. (2013). The evolution of sediment source fingerprinting investigations in fluvial systems. *Journal of Soils and Sediments, 13*(10), 1658–1675.

Walling, D. E., He, Q., & Appleby, P. G. (2002). Conversion models for use in soil-erosion, soil redistribution and sedimentation investigations. Chap. 7. In F. Zapata (Ed.), *Handbook for the assessment of soil erosion and sedimentation using environmental radionuclides* (pp. 111–164). Dordrecht, the Netherlands: Kluwer Ac. Publ.

Wang, J., Huang, T., Wu, Q., Bu, C., & Yin, X. (2021). Sources and cycling of phosphorus in the sediment of rivers along a eutrophic lake in China indicated by phosphate oxygen isotopes. *Acs Earth and Space Chemistry, 5*(1), 88–94.

Wang, J., Zhao, Q., Pang, Y., & Hu, K. (2017). Research on nutrient pollution load in Lake Taihu, China. *Environmental Science and Pollution Research International, 24*(21), 17829–17838.

Wei, Z., Shaoming, P., Kexin, Z., Liguo, C., & Jie, Z. (2015). Study of the cesium-137 reference inventory in the Mainland of China. *Acta Geographica Sinica, 70*(9), 1478–1490.

Wei, Z., Xiaowen, T., Shengtan, S., Zhiqiang, W., & Tianhang, L. J. N. S. G. (2021). Magnetic properties of the surface sediments from the Huguangyan Maar Lake in tropical Southern China and the sediment source identification. *Near Surface Geophysics, 19*(6), 661–676.

Winogradow, A., & Pempkowiak, J. (2020). Identifying recent sources and fate of sedimentary nitrogen in the Baltic Sea based on organic matter elemental composition and nitrogen and carbon stable isotopes ratios. *Marine Pollution Bulletin, 160*, Article 111622.

Wu, L., Liu, X., & Ma, X. Y. (2016). Spatio-temporal variation of erosion-type non-point source pollution in a small watershed of hilly and gully region, Chinese Loess Plateau. *Environmental Science and Pollution Research, 23*(11), 10957–10967.

Xie, H., Huang, Y., Choi, Y., & Shi, J. (2021). Evaluating the sustainable intensification of cultivated land use based on emergy analysis. *Technological Forecasting and Social Change, 165*.

Yang, S., Han, R., Xing, L., Liu, H., Wu, H., & Yang, Z. (2018). Effect of slope farmland soil and water and soil nitrogen and phosphorus loss based on different crop and straw applications and ridge patterns in the basin of the main stream of the Songhua River. *Acta Ecologica Sinica - International Journal, 38*(1), 42–47.

Yan, X., Jiao, J., Tang, B., Liang, Y., & Wang, Z. (2022). Assessing sediment connectivity and its spatial response on land use using two flow direction algorithms in the catchment on the Chinese Loess Plateau. *Journal of Mountain Science, 19*(4), 1119–1138.

Zhang, Y., Jiao, J., Chen, Y., & Tang, B. (2019). Channel morphology and sediment connectivity of fangta watershed in Ansai county of northern shaanxi province. *Research of Soil and Water Conservation, 26*(3), 11–15.

Zhao, Y., Yue, J. H., Xu, C. H., Du, C. G., & Chang, Y. C. (2005). Application of ^{137}Cs tracer technique to estimate the wind erosion rate of Castanozem in Luanhe River Source Area. *Acta Scientiae Circumstantiae, 25*(4), 562–566.